

https://dspace.org/

Synthetic spin dynamics with Bessel-Gaussian optical skyrmions

Singh, Keshaan; Ornelas, Pedro; Dudley, Angela; Forbes, Andrew

2023-05
Optica Publishing Group
https://hdl.handle.net/10539/50217
Singh, K., Ornelas, P., Dudley, A., & Forbes, A. (2023). Synthetic spin dynamics with Bessel-Gaussian optical skyrmions. Optics express, 31(10), 15289–15300. https://doi.org/10.1364/OE.483936

Downloaded from a DSpace repository. https://dspace.org/

Research Article | Vol. 31, No. 10 / 8 May 2023 / Optics Express 15289
Optics EXPRESS

Synthetic spin dynamics with Bessel-Gaussian optical skyrmions

KESHAAN SINGH,* PEDRO ORNELAS, ANGELA DUDLEY, AND ANDREW FORBES

School of Physics, University of the Witwatersrand, Private Bag 3, Johannesburg 2050, South Africa
*keshaanSingh@gmail.com

Abstract: Skyrmions are topologically stable fields that cannot be smoothly deformed into any other field configuration that differs topologically, that is, one that possesses a different integer topological invariant called the Skyrme number. They have been studied as 3-dimensional and 2-dimensional skyrmions in both magnetic and, more recently, optical systems. Here, we introduce an optical analogy to magnetic skyrmions and demonstrate their dynamics within a magnetic field. Our optical skyrmions and synthetic magnetic field are both engineered using superpositions of Bessel-Gaussian beams, with time dynamics observed over the propagation distance. We show that the skyrmionic form changes during propagation, exhibiting controllable periodic precession over a well defined range, analogous to time varying spin precession in homogeneous magnetic fields. This local precession manifests as the global beating between skyrmion types, while still maintaining the invariance of the Skyrme number, which we monitor through a full Stokes analysis of the optical field. Finally, we outline, through numerical simulation, how this approach could be extended to create time varying magnetic fields, offering free-space optical control as a powerful analogue to solid state systems.

© 2023 Optica Publishing Group under the terms of the Optica Open Access Publishing Agreement

1. Introduction

Skyrmions are topologically stable vector-field configurations which were initially proposed to explain strong force phenomena [1–4]. Observations of these structures in magnetic electron-spin systems have received increasing interest due to their superior stability, making them enticing candidates for spintronic information transfer [5–10]. In parallel, optical realizations of skyrmion quasi-particles have garnered much interest in recent years as non-trivial topologically structured light in both classical and quantum regimes [11–15], and have found applications in areas such as optical communication [16,17] and particle trapping [18–20], with new advancements being made in tuning topological degrees of freedom [21–24]. Observations of skyrmion-like structures in the optical-spin of evanescent waves [25] and focused propagating waves carrying orbital angular momentum revealed that the structures can exist at sub-wavelength scales [26]. In condensed matter systems skyrmions have been observed in plasmonic lattices and exiton-polaritons [27,28]. It has been shown that full Poincaré beams [29,30] contain transverse Stokes vector (i.e., psuedospin) distributions which satisfy the topological conditions for 2-dimensional skyrmions [31–33], a distribution formed by the map from the infinite plane, $\mathbb{R}^2 \cup \{\infty\}$, to the sphere, $\mathbb{S}^2$, and are consequently referred to as optical skyrmions [34,35]. These optical skyrmions are commonly constructed using orthogonally polarized Laguerre-Gaussian (LG_p^l) beams (having asymmetric azimuthal indices l, with unequal absolute values). A mechanism for full parametric tuning between skyrmion types such as Néel, Bloch, and anti, which have respective diverging, spiraling and hyperbolic textures, has also been demonstrated [21]. Tracking the trajectories of individual psuedospin states with propagation also revealed mapping to the 4-dimensional hypersphere, which the full Skyrme field maps to, through a Hopf fibration [36–38].

Here, we demonstrate how Bessel-Gaussian (BG_l) beams can be used to engineer optical skyrmions. This is achieved by superimposing two orthogonally polarized BG_l beams of different

#483936 https://doi.org/10.1364/OE.483936
Journal © 2023 Received 21 Dec 2022; revised 22 Feb 2023; accepted 27 Feb 2023; published 24 Apr 2023

Optics EXPRESS

order l, which ensures that all possible relative phases and amplitudes between the beams occur along their transverse profile. The relative phases are imposed along the azimuthal coordinate, φ, by the differing helical phases $e^{il\varphi}$ while the relative amplitudes are achieved in the radial direction by the differing distributions of Bessel functions $J_l()$ having different orders. The resulting distribution of Stokes (i.e., psuedospin) vectors have global topologies which are conveniently confined to a finite on-axis region. We then reveal how the engineered difference between continuously variable radial k_r and axial k_z wavevector components can be used to control the periodic precessional beating of local Stokes vectors. This linear beating with propagation is the result of the Gouy phase difference between the two beams, which is proportional to the difference in k_z. The global effect of the local precession of psuedospins is a change in skyrmion texture with propagation, while preserving the Skyrme number. We then show analytically and by numerical simulation that superpositions of BG_l beams forming optical frozen-waves can be used to engineer psuedospin vectors which, in addition to precession about the polar axis of the Poincaré sphere, also trace a trajectory between the poles. This level of control over propagation dynamic pseudospin trajectory forms a powerful analogy to temporal dynamics of magnetic spin systems in the presence of effective magnetic fields, which can be understood using the Maxwell-Schrödinger formalism. A strong similarity can be drawn to temporal dynamics of psuedospin states in polariton condensates, where the physical mechanism inducing the precession is transverse-electric and transverse-magnetic mode splitting which is also modelled using effective magnetic fields [39]. Another phenomenon, also found in polariton condensates, which shares similarities with our free-space work is the Rabi trajectories of quantum state vectors on the Bloch-Sphere [40]. This highlights how the analogy can extend beyond spin/polarization states to spatial/Bloch states. This connection between the optical and solid-state regimes allows for the powerful free-space optical toolkit to be applied in understanding dynamics of more complex systems, treating the optical skyrmions as quasi-particles with stability imbued courtesy of their topological soliton nature.

2. Theory

Consider the superposition of two BG_l beams in the orthogonal right-circular (left-circular) $R(L)$ polarization basis

$$|\Psi\rangle = \mathrm{BG}_{l_R}(r, \varphi, z, k_z^R)|R\rangle + \mathrm{BG}_{l_L}(r, \varphi, z, k_z^L)|L\rangle, \tag{1}$$

$$BG_l(r, \varphi, z, k_z) = e^{-\frac{r^2}{w_0^2}} J_l(rk_r) e^{il\varphi} e^{ik_z z}, \tag{2}$$

where r, φ and z are the respective radial, azimuthal and axial cylindrical coordinates and $J_l()$ denotes the l^{th} order Bessel function of the first kind. $|R\rangle$ and $|L\rangle$ represent the appropriate polarization Jones vectors, k_z and $k_r = \sqrt{k^2 - k_z^2}$, are the respective axial and radial wavevector components. We use l to label the topological charge and w_0 is the width of the Gaussian amplitude envelope which will be subsequently omitted for brevity. Now let us recall that the Skyrme field components Σ_i are given by [34]

$$\Sigma_i(x, y, z) = \epsilon_{ijk}\epsilon_{pqr} S_p \partial_j S_q \partial_k S_r, \tag{3}$$

where $(i, j, k) = (x, y, z)$ and $(p, q, r) = (1, 2, 3)$, $S_p(x, y, z)$ are the (locally normalized) Stokes parameters (where we have omitted the spatial dependence for brevity) and $\epsilon_{ijk(pqr)}$ are the Levi-Cevita permutation operators. If we confine ourselves to a single transverse plane (e.g.,

Optics EXPRESS

$z = 0$), we can calculate the field's Skyrme number, $\mathcal{N}$, as

$$\mathcal{N} = \frac{1}{4\pi}\int_0^{\infty}\int_0^{2\pi}\Sigma_z(r\cos\varphi, r\sin\varphi)d\varphi dr, \tag{4}$$

where the Σ_z component of the Skyrme field is given by

$$\begin{aligned}\Sigma_z(r\cos\varphi, r\sin\varphi) = \Sigma_z(x,y) = {} & S_1\partial_x S_2\partial_y S_3 + S_2\partial_x S_3\partial_y S_1 + S_3\partial_x S_1\partial_y S_2 \\ & -(S_1\partial_x S_3\partial_y S_2 + S_2\partial_x S_1\partial_y S_3 + S_3\partial_x S_2\partial_y S_1)\,.\end{aligned} \tag{5}$$

Note that we choose to define Σ_z in cartesian coordinates (as this correlates better with experimentally acquired CCD images), while the integral is performed in polar coordinates to exploit the cyrlindrical symmetry of the fields. It can be shown that by exploiting the cylindrical symmetry of the Bessel-Gaussian modes, the above calculation yields the following simplified integral [21,41]

$$\mathcal{N} = q\Delta\ell\int_0^{\infty} g(\alpha)dr \tag{6}$$

where $g(\alpha) = \frac{\partial\alpha^2}{\partial r}\frac{1}{(1+\alpha^2)^2}$, $\alpha(r) = \left|J_{l_L}(rk_r)\right|^q\left|J_{l_R}(rk_r)\right|^{-q}$, $\Delta\ell = \ell_R - \ell_L$ with $|\ell_R| \neq |\ell_L|$ and $q = \frac{|\ell_L|-|\ell_R|}{||\ell_L|-|\ell_R||}$. It is clear then for the roots of the lower order Bessel function, we have that $\alpha \to \infty$. This then means that α is only continuous in the domains $(0, r_0)\bigcup_{i=0}^{\infty}(r_i, r_{i+1})$, where $r_i \in \mathbb{R}$ are the roots of the lower order Bessel function. As such, to evaluate Eq. (6) such that we obtain an integer Skyrme number, we choose to break up the integral as follows

$$\mathcal{N} = q\Delta\ell\left[\int_0^{r_0} g(\alpha)dr + \sum_{i=0}^{\infty}\int_{r_i}^{r_{i+1}} g(\alpha)dr\right], \tag{7}$$

which can then be evaluated to give

$$\mathcal{N} = q\Delta\ell\left[\left(\frac{1}{1+\alpha(0)^2} - \frac{1}{1+\alpha(r_0)^2}\right) + \sum_{i=0}^{\infty}\left(\frac{1}{1+\alpha(r_i)^2} - \frac{1}{1+\alpha(r_{i+1})^2}\right)\right]. \tag{8}$$

Clearly the second term in Eq. (8) will always evaluate to zero unless the two Bessel functions share roots. However, this is not the case, as according to Bourgat's Hypothesis [42], Bessel functions of varying positive orders do not have any roots in common. And so we are left with

$$\mathcal{N} = q\Delta\ell\left(\frac{1}{1+\alpha(0)^2} - \frac{1}{1+\alpha(r_0)^2}\right), \tag{9}$$

which analytically indicates that the generated state given in Eq. (1) has a skyrmionic topology in the localized region $(0, r_0)$. From the definition given to α, it is clear that the term within the brackets will always evaluate to an integer as $\alpha(r)$ can only tend to either 0 or ∞ at both $r = 0$ and $r = r_0$ which implies that our field is in fact skyrmionic. Furthermore, since the ratio given in the definition of α inverts depending on the sign of q, we have that the first term in the brackets always evaluates to 1 while the second always evaluates to 0, as such the Skyrme number in this central region is easily controlled by modifying q and $\Delta\ell$, which independently control the polarity [21] (affected by which component in Eq. (1) dominates at $r = 0, r_0$.) and the order/vorticity [21] of the Skyrme number. A truncated segment of the Skyrme field, Σ_z, is shown in Fig. 1(a), where we can see that the central region's Skyrme number evaluates to 1, whereas the Skyrme number in concentric annulus regions around the origin evaluate to 0. By subdividing each of these outer annulus regions into regions where the function $\zeta = \alpha + \alpha^{-1}$ is continuous, we obtain Skyrme number contributions of $\mathcal{N}$ and $-\mathcal{N}$ which compensate for one

Optics EXPRESS

another thereby yielding an effective skyrmion contribution of 0. This is evident in Fig. 1(a) where each concentric annulus ring can clearly be divided into two annulus rings which contribute only positive or negative values to the Skyrme field, Σ_z. Physically this phenomenom can be seen as wrapping around the Poincaré sphere and then unwrapping again within the same region. This, along with the approximately non-diffracting nature of BG_l beams, allows for a more practical implementation than the infinite bounds required by LG_p^l skyrmions. We note that the above analysis has been done for $k_z^R = k_z^L$, however as long as for $k_z^R \neq k_z^L$, the first zeroes do not overlap, then Eq. (9) will still evaluate to an integer, thereby forming a skyrmionic topology which wraps the Poincaré sphere $\mathcal{N}$ times. For practical purposes, we do require that the zeroes of the Bessel functions be sufficiently far apart.

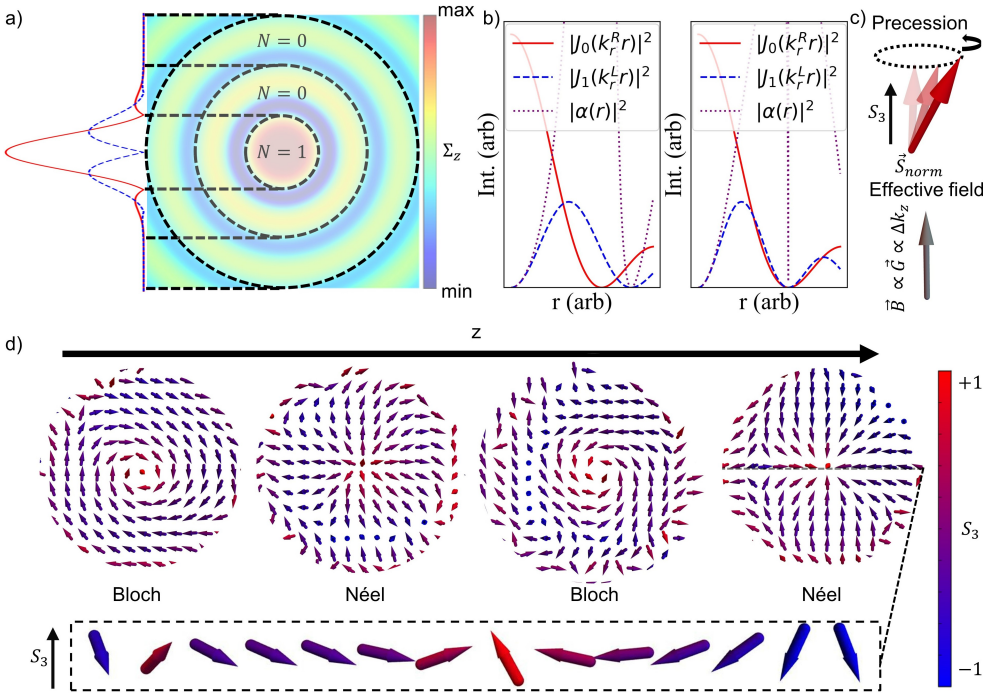


Fig. 1. a) Left: Overlayed theoretical intensity plot of constituent orthogonally polarized Bessel modes as shown by the dashed rings. Right: Skyrme field with Skyrme number $\mathcal{N}$ associated to the concentric annular regions placed as insets. b) Theoretical plots of the relative intensity of the constituent BG_l components ($l_R = 0$, $l_L = 1$) for valid ($k_r^L = 1.2k_r^R$) and invalid ($k_r^L = 1.6k_r^R$) choice of radial wavevectors, where $|\alpha(r)|^2 = |J_{l_L}(k_r^L r)|^{2q}|J_{l_R}(k_r^R r)|^{-2q}$ with q defined in the text. c) Conceptual illustration of local Stokes vector precession about the S_3 axis due to the effective inhomogeneity $\vec{G}$ caused by the Gouy-phase difference between orthogonally polarized constituents. d) Experimentally measured vector plots of BG_l optical skyrmions beating between continuously deformable Bloch- and Néel-types, as well as a section indicating the radial variation of S_3.

In Fig. 1(b), we show theoretical plots of relative intensities of the orthogonally polarized components for valid and invalid choices of $k_r^{R(L)}$. An invalid choice is characterized by values of $k_r^{R(L)}$ which result in $J_{l_R(l_L)}(k_r^{R(L)}r)$ distributions with first minima (excluding those at $r = 0$) which overlap. An overlap will result in a pseudospin field which does not map to the complete Poincaré sphere, and therefore does not constitute a skyrmion.

Optics EXPRESS

The Stokes parameters of our vector beam are calculated using Pauli matrices σ_p - and $\sigma_0 = \mathcal{I}$ as $S_p = \langle\Psi|\sigma_p|\Psi\rangle$, resulting in

$$S_0 = |J_{l_R}(rk_r^R)|^2 + |J_{l_L}(rk_r^L)|^2, \tag{10}$$

$$S_1 = 2J_{l_R}(rk_r^R)J_{l_L}(rk_r^L)\cos(\Delta l\varphi + \Delta k_z z), \tag{11}$$

$$S_2 = -2J_{l_R}(rk_r^R)J_{l_L}(rk_r^L)\sin(\Delta l\varphi + \Delta k_z z), \tag{12}$$

$$S_3 = |J_{l_R}(rk_r^R)|^2 - |J_{l_L}(rk_r^L)|^2, \tag{13}$$

where $\Delta l = l_R - l_L$ and $\Delta k_z = k_z^R - k_z^L$. From Eqs. (10) to (13) we can see that each local transverse Stokes vector [i.e., fixed $\vec{r}_T = (r, \varphi)$] will experience a periodic precession about the S_3 axis proportional to Δk_z as the vector field propagates. Important cases are where $r = 0$ and $r = r_0$ where we get $S_3 = \pm 1$, which is constant with z. It is also notable that due to the relationship $k_r = \sqrt{k^2 - k_z^2}$, either $\Delta k_r = k_r^R - k_r^L$ or Δk_z could be used to tune the precession rate. The linear Gouy phase of our BG$_l$ beams allow for true periodic beating between (continuously deformable) skyrmion types over a well defined distance, which differs from the asymptotic arctan behaviour of conventional free-space LG$_p^l$ optical skyrmion dynamics. It can be noted that in polariton condensates periodic trajectories of state/pseudospin vectors has been realized through various mechanisms [39,40]. It should also be noted that Eqs. (12) and (13) experience symmetry under the interchange of z and ϕ which means that complete precession leads to skyrmion textures in planes orthogonal to the propagation direction. This can be seen by taking a plane at a fixed azimuthal angle and projecting it along r and z until the radial bound for the skyrmion and the axial bound of one complete pseudospin precession respectively. This results in a skyrmion texture in rectangular planes orthogonal to the beam axis for all azimuthal angles. To draw a comparison to anisotropic optical systems we can adopt the Maxwell-Schrödinger formalism, which describes pseudospin transformations of light propagating in anisotropic media and reveals the equation of motion [43]

$$\lambda\frac{\partial\vec{S}}{\partial z} = \vec{S}\times\vec{G}\,. \tag{14}$$

Here λ is the wavelength, $\vec{S} = S_0^{-1}(S_1, S_2, S_3)^T$ is the locally normalized Stokes vector and $\vec{G} = (2\alpha, 2\beta, 2\gamma)^T$ is the vector describing the anisotropic medium. The parameters α, β and γ specify the axes of linear birefringence, the retardance between this axes and the retardance between pure circular polarizations respectively. In the case we have been examining, we observe a pseudospin evolution in free-space when $\alpha = \beta = 0$ and $\gamma = \frac{1}{2}\lambda\Delta k_z$. A resemblance between Eq. (14) and the temporal equation of motion of a magnetic spin system in a magnetic field is clear, where λ plays the role of Planck's constant and $\vec{G}$ resembles an applied magnetic field [43]. A schematic illustrating the Larmor-like precession of the normalized Stokes vector about the $\vec{G}$ axis is included in Fig. 1(c). In order to further highlight the value of the free-space optical analogy (beyond static homogeneous $\vec{G}$ fields), we can utilize so-called optical frozen waves (FWs) which are constructed using superpositions of BG$_l$ beams given by [44,45]

$$\mathrm{FW}(r, z, f(z), Q) = e^{iQz}\sum_{n=-N}^{N} A_n(f(z))J_0(k_{r,n}r)e^{i\frac{2\pi}{L_{FW}}nz}, \tag{15}$$

$$An = \frac{1}{L_{FW}}\int_0^{L_{FW}} f(z)e^{-i\frac{2\pi}{L_{FW}}nz}dz\,. \tag{16}$$

Here Q is the 'central' k_z about which the superposition is constructed, $2N + 1$ is the number of BG_l modes in the superposition and $f(z)$ is an arbitrary function which the central intensity of

Optics EXPRESS

the FW will approximate (i.e., $|\mathrm{FW}(0,z,f(z))|^2 \approx |f(z)|^2$). L_{FW} is the propagation distance over which the FW is defined. We can use these FWs as the constituent components of our vector field

$$|\Psi\rangle = \mathrm{FW}(r,z,f^R(z),Q_R)|R\rangle + \mathrm{FW}(r,z,f^L(z),Q_L)|L\rangle\,. \tag{17}$$

By choosing $Q_R \neq Q_L$ with an appropriate choice of $f^{R(L)}(z)$, we can have an on-axis (i.e., $r = 0$) Stokes vector which, in addition to the precession about S_3, can trace paths between the poles of the Poincaré sphere. As an example we can consider $f^R(z) = \sqrt{z/L_{FW}}$ and $f^L(z) = \sqrt{1 - z/L_{FW}}$ resulting in Stokes parameters approximated by

$$S_0 \approx 1, \tag{18}$$

$$S_1 \approx 2\sqrt{\frac{z}{L_{FW}}}\sqrt{1-\frac{z}{L_{FW}}}\cos(\Delta k_z z), \tag{19}$$

$$S_2 \approx -2\sqrt{\frac{z}{L_{FW}}}\sqrt{1-\frac{z}{L_{FW}}}\sin(\Delta k_z z), \tag{20}$$

$$S_3 \approx \frac{2z}{L_{FW}} - 1\,. \tag{21}$$

We then model axially dependent $\vec{G}$, analagous to a time-varying $\vec{B}$ field , in free-space

$$\vec{G}(z) \approx \begin{pmatrix} \frac{\sin(\Delta k_z z)}{L_{FW}\sqrt{\frac{z}{L_{FW}}}\sqrt{1-\frac{z}{L_{FW}}}} \\ \frac{\cos(\Delta k_z z)}{L_{FW}\sqrt{\frac{z}{L_{FW}}}\sqrt{1-\frac{z}{L_{FW}}}} \\ \frac{(L_{FW}-2\Delta k_z(z-1)z-2z)\cot(\Delta k_z)+L_{FW}-2z}{2z(L_{FW}-z)} \end{pmatrix}. \tag{22}$$

The case of FWs is distinct from the case of optical skyrmions as the control is over a single on-axis pseudospin vector as opposed to a transverse distribution of pseudospins, our implementation of FWs serves as a first step toward the use of spatially varying FWs which could exhibit changes of not only skyrmion textures but also Skyrme number during propagation [46,47]. It should be noted that while FWs have been generated experimentally, the large range of k_z values required to accurately approximate $f(z)$ creates some requirements for large system apertures to acquire this. Due to these restrictions our demonstration of pseudospin control using FWs is based on simulations involving propagating the field using numerical angular spectrum propagation [48].

3. Experiment

To investigate the predicted behaviour of the vector fields described in Sec. 2, we used the arrangement shown in Fig. 2. A horizontally polarized Gaussian beam from a HeNe laser (operating at a wavelength of $\lambda = 632.5$ nm) was expanded and collimated using lenses EL ($f = 2$ mm) and CL ($f = 250$ mm) respectively, such that the central transverse region of the beam approximated a plane wave of constant amplitude. The expanded beam then had its polarization axis rotated by 45° with a half-wave plate (HWP) before it was passed through a Wollaston prism (WP) and quater-wave plate (QWP) which separated the right- (R) and left-circularly (L) polarized components of the expanded beam by an angle of $\approx 1°$ (in the horizontal $x - z$ plane). A $4f$ system was then used to image the plane at the WP onto the screen of a digital micro-mirror

Optics EXPRESS

device (DMD, TI-DLP6500). To facilitate complex amplitude modulation of the incident light [49], we make use of two binary amplitude holograms of the form

$$H_{A(B)}(\vec{r}) = \frac{1}{2} - \frac{1}{2}\left(\cos(\pi\Phi(\vec{r}) + 2\pi\vec{g}^{A(B)} \cdot \vec{r}) + \cos(\pi A(\vec{r}))\right), \tag{23}$$

which were multiplexed and displayed by the DMD. We define $\vec{r} = (x, y)$ as the Cartesian pixel coordinates, $\Phi(\vec{r}) = \frac{\arg(T^{A(B)}(\vec{r}))}{\pi}$ and $A(\vec{r}) = \frac{\arcsin(|T^{A(B)}(\vec{r})|)}{\pi}$ are the re-normalized phases and amplitudes of the complex transmission functions $T^{A(B)}(\vec{r})$. With the 0^{th} diffraction orders of the $R(L)$ components leaving the DMD screen at the same 1° separation angle, the spatial carrier frequencies $\vec{g}^{A(B)} = (g_x^{A(B)}, g_y^{A(B)})$ were chosen such that the 1^{st} diffraction order containing the complex field distributions $T^A(\vec{r})$ in the R polarization spatially overlapped (co-linearly) with the 1^{st} order of the $T^B(\vec{r})$ distribution in the L polarization [50]. It should be noted that the resulting gratings have spatially constant frequencies (for each hologram $H_{A(B)}$), with local shifts in the fringes associated with the desired phase modulation [51]. Finally a Fourier lens (F: $f = 0.2$ m) was used to project the far-field intensity onto a CCD camera. The transmission functions were set according to $T^{A(B)}(\vec{r}) = \mathcal{F}\{\langle R(L)|\Psi\rangle_{z=0}\}e^{iq_z(q_x,q_y)z}$, where $\mathcal{F}\{\}$ represents the Fourier transform, $q_z(q_x, q_y)$ is the spatially varying transverse angular spectrum used to digitally propagate the field captured at the CCD by the distance z [52]. A QWP and linear polarizer (LP) were used to project Stokes intensities of the generated fields onto the CCD [53]. It is notable that the digital propagation scheme should result in similar results to those which could be obtained by physically translating the CCD along z. The digital scheme was preferable as it allowed for automated measurements and for the Stokes intensities to be more accurately aligned since there was no risk of the CCD shifting.

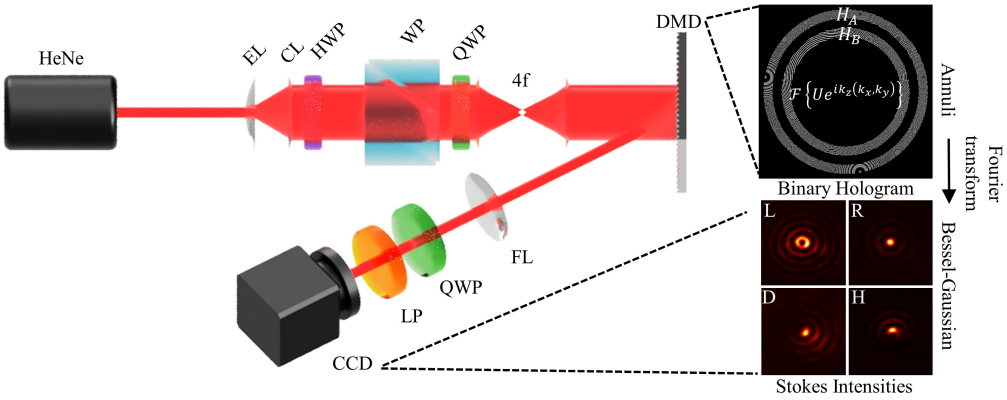


Fig. 2. Diagram showing the experimental arrangement used to generate and analyse BG_l based optical skyrmions [WP - Wollaston prism, EL - expansion lens, CL - collimation lens, HWP - half-wave plate, QWP - quater-wave plate, DMD - digital micro-mirror device, FL - Fourier lens, LP - linear polarizer]. The top right inset shows an example of binary amplitude holograms featuring individual rings for each of the two multiplexed holograms $H_{A(B)}$ (far-field). The bottom right inset shows examples of Stokes intensities measured by the CCD (near-field).

4. Results and discussion

Using the arrangement in Sec. 3, we generated vector fields of the form in Eq. (1). We set the parameters $l_R = 0$, $l_L = [1, -2, 3]$ and $k_z^{R(L)} = 0.999995(0.999986)k$. Using Stokes intensity measurements of the R, L, D (diagonal) and H (horizontal) polarization projections, we extracted

Optics EXPRESS

the transverse Stokes vector distribution at 26 evenly spaced planes over the digitally propagated range $z \in [-0.9, 0.9]$ m. In Fig. 1(d) we show the experimentally measured Stokes vector fields of the case with $l_L = 1$ at various planes where the transition between Bloch- and Néel-type

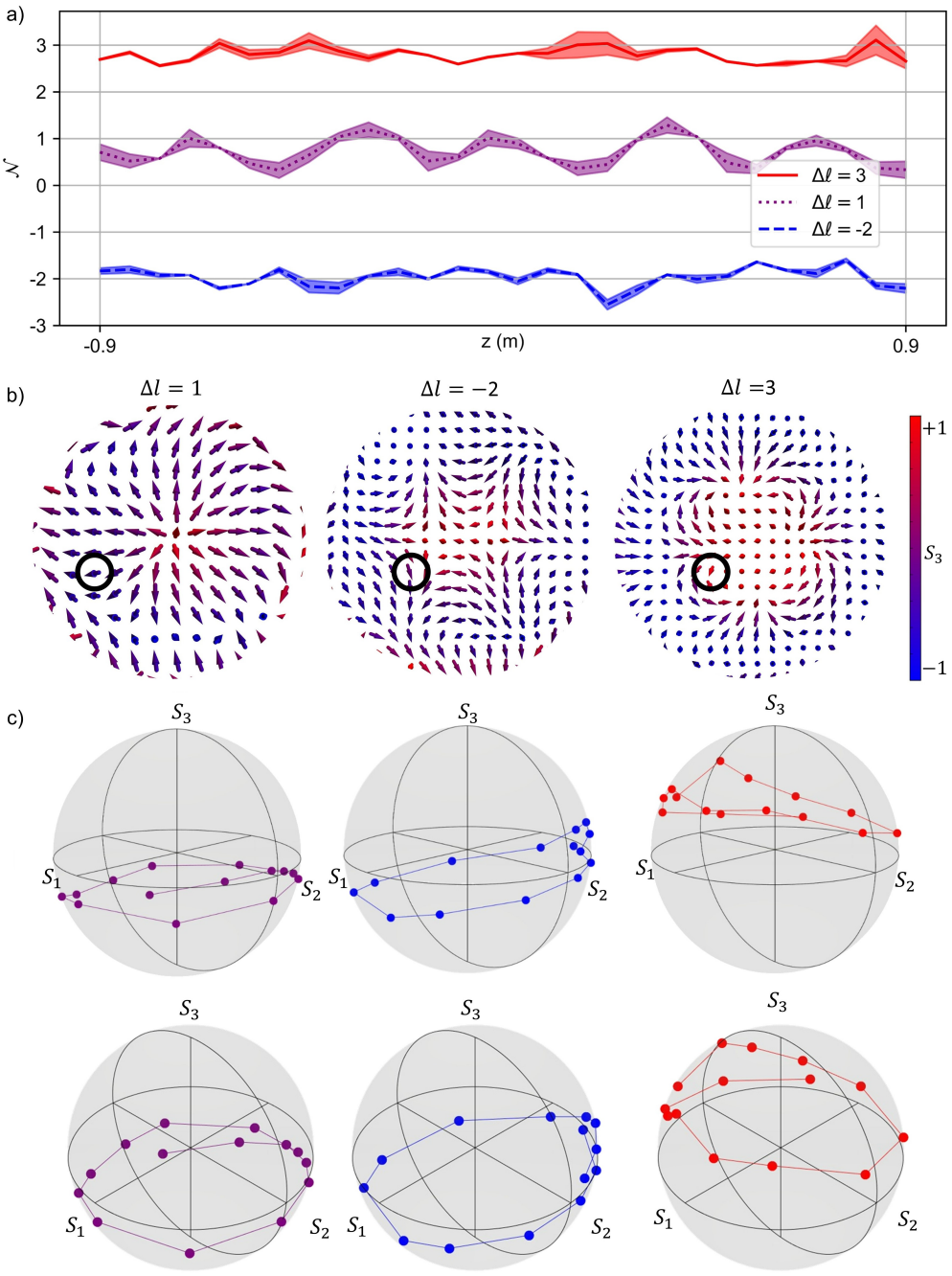


Fig. 3. a) Plot showing the experimentally measured Skyrme number of various BG_l optical (anti-)skyrmions propagated over a well defined distance. b) Experimentally measured Stokes vector fields of the corresponding BG_l skyrmions in a). c) Plots showing the experimentally measured precession of a local Stokes vectors (from the corresponding beams of a) about the S_3 axis with propagation for various $\mathcal{N}$.

Optics EXPRESS

skyrmions, characterized by the respective 'hedgehog' and 'spiral' textures, is clear. Inspection of the local behaviour of individual vectors reveals the precessional dynamics akin to that of anisotropic and magnetic systems. In Fig. 3(a) we show how the topological index of $\mathcal{N}$ is preserved over the propagation range, here $\mathcal{N}$ was calculated using Eq. (4) where the transverse gradients were determined using a numerical second-order finite difference approximation, while the error-bands were calculated by propagating the observed 2 % shot noise through Eq. (4). Notwithstanding the visible fluctuations in the approximated $\mathcal{N}$, the invariance of the distinct values with propagation is evident. The cause of the excessive fluctuations in the $l_L = 1$ case is due to the effect of rapidly changing relative amplitudes for lower order skyrmions, which induce errors in the computation method used to calculate gradients. The invariance of the Skyrme number highlights the stability of the structures to the effect of the $\vec{G}$ fields in the Maxwell-Schrödinger formalism. Plots of the locally normalized Stokes vector fields (sampled at every 3 pixels of the measured data) for various Δl are shown in Fig. 3(b) where the azimuthally varying vector orientations give the characteristic textures associated which each Skyrme number. In Fig. 3(c) we show plots of the paths, on the Poincaré sphere, traced by sample Stokes vectors (at the positions indicated in Fig. 3(b)). The predicted complete rotation of the local vectors about the S_3 axis over a finite distance is clear, it is notable that to observe a complete rotation utilizing LG_p^l modes one would need to observe the field propagation to infinity. In Fig. 4(a) we show the numerically simulated spiraling path traced out by the central Stokes vector of a field taking the form in Eq. (17), modeling the dynamics of an electron spin/Stokes vector and a magnetic field/anisotropic material of the form in Eq. (22). The dynamics were simulated over a 200 mm distance with $Q_R(L) = (0.99997)0.99985$. We can note that the path deviates from an ideal spiral at the poles, this is due to the approximate nature of the FW which is highlighted when comparing the simulated relative phase and amplitude to the ideal case shown in Fig. 4(b). This system emulates a dynamic applied magnetic field or, equivalently an axially dependent anisotropic material which results in a (pseudo)spin state which accesses a large portion of possible orientations over a well defined propagation length. It is also notable that this propagation dynamic trajectory is similar to that observed in time dynamic Bloch vectors which

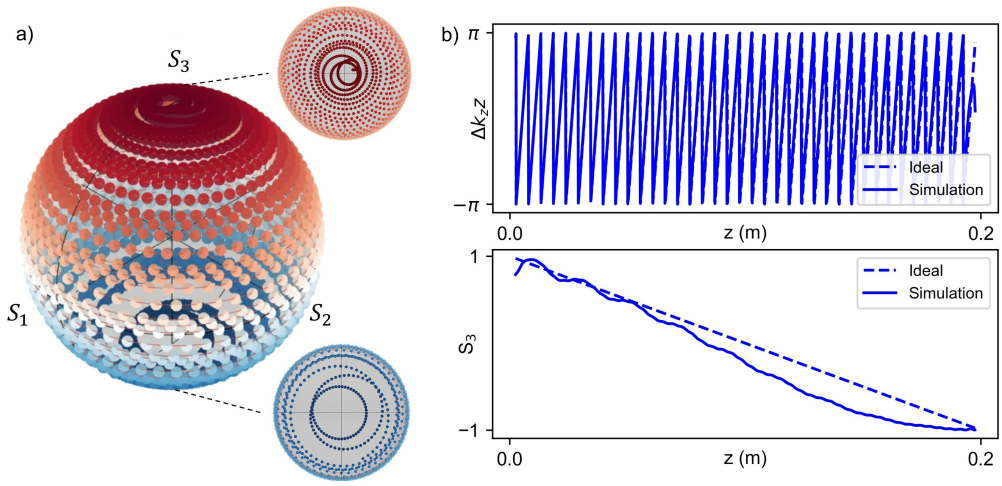


Fig. 4. a) Plot showing the path traced during propagation of a numerically simulated central ($r = 0$) Stokes vector generated using optical 'frozen-waves', insets show the views from each of the poles. b) Plots showing the ideal (theoretical) and simulated (via the angular spectrum method) relative phase $\Delta k_z z$ and amplitude S_3 of the constituent components of the vector field used to produce the Stokes vector rotation in (a).

Optics EXPRESS

evolve in polariton condensates [40]. This extension of the Maxwell-Schrödinger formalism, which is generally restricted to anisotropic media, to the realm of free-space optics provides a more accessible form of the analogy [43].

5. Conclusions

We have generated and analysed a variation of skyrmions in the Stokes field engineered using BG_l beams, with different absolute values in their l indices. We have shown how the global topological invariant can be extracted from a finite region and how unequal axial wavevector components in the constituent beams lead to precessional dynamics of pseudospins which cause a global transformation between Bloch and Néel type skyrmions with different initial angles. We experimentally verify the invariance of the topological index of the generated fields with propagation. We also propose a technique to extend the optical control of psuedospin dynamics by exploiting optical frozen-waves constructed by superpositions of BG_l beams. We show how these propagation dynamics of pseudospin states are analogous to time dynamics of magnetic spin states, where the skyrmion beating is characteristic of behaviour in a static magnetic field and the frozen-wave case allows for dynamic magnetic fields to be emulated. The analogy can be described using the Maxwell-Schrödinger formalism, which often relates optical propagation through anisotropic media to magnetic systems. Further work exploiting spatially structured frozen-waves, could see Stokes vector fields with Skyrme numbers which change with propagation, analogous to temporal dynamics of spin systems in applied magnetic fields which vary spatially and temporally [46,47].

Funding. Department of Science and Innovation, South Africa.

Acknowledgments. The authors acknowledge support from the Department of Science and Innovation, South Africa.

Disclosures. The authors declare no conflicts of interest.

Data availability. Data underlying the results presented in this paper are not publicly available at this time but may be obtained from the authors upon reasonable request.

References

1. T. H. R. Skyrme, "A unified field theory of mesons and baryons," Nucl. Phys. **31**, 556–569 (1962).
2. I. Zahed and G. Brown, "The skyrme model," Phys. Rep. **142**(1-2), 1–102 (1986).
3. C. Naya and P. Sutcliffe, "Skyrmions and clustering in light nuclei," Phys. Rev. Lett. **121**(23), 232002 (2018).
4. J. Eisenberg and G. Kälbermann, "The use of skyrmions for two-nucleon systems," Progress in Particle and Nuclear Physics **22**, 1–42 (1989).
5. X. Yu, Y. Onose, N. Kanazawa, J. H. Park, J. Han, Y. Matsui, N. Nagaosa, and Y. Tokura, "Real-space observation of a two-dimensional skyrmion crystal," Nature **465**(7300), 901–904 (2010).
6. A. Fert, V. Cros, and J. Sampaio, "Skyrmions on the track," Nat. Nanotechnol. **8**(3), 152–156 (2013).
7. A. Fert, N. Reyren, and V. Cros, "Magnetic skyrmions: advances in physics and potential applications," Nat. Rev. Mater. **2**(7), 17031–15 (2017).
8. N. Nagaosa and Y. Tokura, "Topological properties and dynamics of magnetic skyrmions," Nat. Nanotechnol. **8**(12), 899–911 (2013).
9. X. Zhang, Y. Zhou, K. M. Song, T.-E. Park, J. Xia, M. Ezawa, X. Liu, W. Zhao, G. Zhao, and S. Woo, "Skyrmion-electronics: writing, deleting, reading and processing magnetic skyrmions toward spintronic applications," J. Phys.: Condens. Matter **32**(14), 143001 (2020).
10. I. Lima Fernandes, S. Blügel, and S. Lounis, "Spin-orbit enabled all-electrical readout of chiral spin-textures," Nat. Commun. **13**(1), 1576 (2022).
11. M. Soskin, S. V. Boriskina, Y. Chong, M. R. Dennis, and A. Desyatnikov, "Singular optics and topological photonics," J. Opt. **19**(1), 010401 (2016).
12. M. R. Dennis, Y. S. Kivshar, M. S. Soskin, and G. A. S. Jr, "Singular optics: more ado about nothing," J. Opt. A: Pure Appl. Opt. **11**(9), 090201 (2009).
13. N. Rivera and I. Kaminer, "Light–matter interactions with photonic quasiparticles," Nat. Rev. Phys. **2**(10), 538–561 (2020).
14. R. Gutiérrez-Cuevas and E. Pisanty, "Optical polarization skyrmionic fields in free space," J. Opt. **23**(2), 024004 (2021).

Optics EXPRESS

15. P. Ornelas, I. Nape, R. D. M. Koch, and A. Forbes, "Non-local skyrmions as topologically resilient quantum entangled states of light," arXiv, arXiv:2210.04690 (2022).
16. J. Wang, J.-Y. Yang, I. M. Fazal, N. Ahmed, Y. Yan, H. Huang, Y. Ren, S. Yue, Y. Dolinar, M. Tur, and A. E. Willner, "Terabit free-space data transmission employing orbital angular momentum multiplexing," Nat. Photonics **6**(7), 488–496 (2012).
17. A. Karnieli, S. Tsesses, G. Bartal, and A. Arie, "Emulating spin transport with nonlinear optics, from high-order skyrmions to the topological hall effect," Nat. Commun. **12**(1), 1092–1099 (2021).
18. K. T. Gahagan and G. A. Swartzlander, "Optical vortex trapping of particles," Summaries of papers presented at the *Conference on Lasers and Electro-Optics* pp. 155–156 (1996).
19. M. Padgett and R. Bowman, "Tweezers with a twist," Nat. Photonics **5**(6), 343–348 (2011).
20. X.-G. Wang, L. Chotorlishvili, V. K. Dugaev, A. Ernst, I. V. Maznichenko, N. Arnold, C. Jia, J. Berakdar, I. Mertig, and J. Barnas, "The optical tweezer of skyrmions," npj Comput. Mater. **6**(1), 140–147 (2020).
21. Y. Shen, E. C. Martínez, and C. Rosales-Guzmán, "Generation of optical skyrmions with tunable topological textures," ACS Photonics **9**(1), 296–303 (2022).
22. Q. Zhang, Z. Xie, L. Du, P. Shi, and X. Yuan, "Bloch-type photonic skyrmions in optical chiral multilayers," Phys. Rev. Research **3**(2), 023109 (2021).
23. Q. Zhang, Z. Xie, P. Shi, H. Yang, H. He, L. Du, and X. Yuan, "Optical topological lattices of bloch-type skyrmion and meron topologies," Photon. Res. **10**(4), 947–957 (2022).
24. H. R. O. Sohn, C. D. Liu, Y. Wang, and I. I. Smalyukh, "Light-controlled skyrmions and torons as reconfigurable particles," Opt. Express **27**(20), 29055–29068 (2019).
25. S. Tsesses, E. Ostrovsky, K. Cohen, B. Gjonaj, N. H. Lindner, and G. Bartal, "Optical skyrmion lattice in evanescent electromagnetic fields," Sciences **361**(6406), 993–996 (2018).
26. L. Du, A. Yang, A. V. Zayats, and X. Yuan, "Deep-subwavelength features of photonic skyrmions in a confined electromagnetic field with orbital angular momentum," Nat. Phys. **15**(7), 650–654 (2019).
27. A. Ghosh, S. Yang, Y. Dai, and H. Petek, "The spin texture topology of polygonal plasmon fields," ACS Photonics **10**(1), 13–23 (2023).
28. T. Byrnes, N. Y. Kim, and Y. Yamamoto, "Exciton–polariton condensates," Nat. Phys. **10**(11), 803–813 (2014).
29. A. M. Beckley, T. G. Brown, and M. A. Alonso, "Full poincaré beams," Opt. Express **18**(10), 10777–10785 (2010).
30. W. Lin, Y. Ota, Y. Arakawa, and S. Iwamoto, "Microcavity-based generation of full poincaré beams with arbitrary skyrmion numbers," Phys. Rev. Research **3**(2), 023055 (2021).
31. L. D. Faddeev and V. E. Korepin, "Quantization of solitons," Theor. Math. Phys. **25**(2), 1039–1049 (1975).
32. R. Battye and P. M. Sutcliffe, "Solitons, links and knots," Proceedings of the Royal Society of London. Series A: Mathematical, Physical and Engineering Sciences **455**(1992), 4305–4331 (1999).
33. N. Manton and P. Sutcliffe, *Topological Solitons*, Cambridge Monographs on Mathematical Physics (Cambridge University Press, 2004).
34. S. Gao, F. C. Speirits, F. Castellucci, S. Franke-Arnold, S. M. Barnett, and J. B. Götte, "Paraxial skyrmionic beams," Phys. Rev. A **102**(5), 053513 (2020).
35. H. Kuratsuji and S. Tsuchida, "Evolution of the stokes parameters, polarization singularities, and optical skyrmion," Phys. Rev. A **103**(2), 023514 (2021).
36. D. Sugic, R. Droop, E. Otte, D. Ehrmanntraut, F. Nori, J. Ruostekoski, C. Denz, and M. R. Dennis, "Particle-like topologies in light," Nat. Commun. **12**(1), 6785 (2021).
37. D. W. Lyons, "An elementary introduction to the hopf fibration," Mathematics Magazine **76**(2), 87–98 (2003).
38. H. Urbantke, "The hopf fibration—seven times in physics," Journal of Geometry and Physics **46**(2), 125–150 (2003).
39. S. Donati, L. Dominici, G. Dagvadorj, D. Ballarini, M. De Giorgi, A. Bramati, G. Gigli, Y. G. Rubo, M. H. Szymańska, and D. Sanvitto, "Twist of generalized skyrmions and spin vortices in a polariton superfluid," Proc. Natl. Acad. Sci. **113**(52), 14926–14931 (2016).
40. L. Dominici, D. Colas, A. Gianfrate, A. Rahmani, V. Ardizzone, D. Ballarini, M. De Giorgi, G. Gigli, F. P. Laussy, D. Sanvitto, and N. Voronova, "Full-bloch beams and ultrafast rabi-rotating vortices," Phys. Rev. Res. **3**(1), 013007 (2021).
41. S. Gao, Skyrmionic beams and quantum matched filtering, Ph.D. thesis, University of Glasgow (2022).
42. G. N. Watson, A treatise on the theory of Bessel Functions (Cambridge University Press, 1922).
43. H. Kuratsuji and S. Kakigi, "Maxwell-schrödinger equation for polarized light and evolution of the stokes parameters," Phys. Rev. Lett. **80**(9), 1888–1891 (1998).
44. M. Zamboni-Rached, "Stationary optical wave fields with arbitrary longitudinal shape by superposing equal frequency bessel beams: Frozen waves," Opt. Express **12**(17), 4001–4006 (2004).
45. M. Zamboni-Rached, E. Recami, and H. E. Hernández-Figueroa, "Theory of "frozen waves": modeling the shape of stationary wave fields," JOSA A **22**(11), 2465–2475 (2005).
46. A. H. Dorrah, M. Zamboni-Rached, and M. Mojahedi, "Controlling the topological charge of twisted light beams with propagation," Phys. Rev. A **93**(6), 063864 (2016).
47. A. H. Dorrah, C. Rosales-Guzmán, A. Forbes, and M. Mojahedi, "Evolution of orbital angular momentum in three-dimensional structured light," Phys. Rev. A **98**(4), 043846 (2018).
48. D. G. Voelz, Computational fourier optics: a MATLAB tutorial, vol. 534 (SPIE press Bellingham, Washington, 2011).

Optics EXPRESS

49. W.-H. Lee, "Binary computer-generated holograms," Appl. Opt. **18**(21), 3661–3669 (1979).
50. C. Rosales-Guzmán, X.-B. Hu, A. Selyem, P. Moreno-Acosta, S. Franke-Arnold, R. Ramos-Garcia, and A. Forbes, "Polarisation-insensitive generation of complex vector modes from a digital micromirror device," Sci. Rep. **10**, 10434 (2020).
51. M. Mirhosseini, O. S. Magana-Loaiza, C. Chen, B. Rodenburg, M. Malik, and R. W. Boyd, "Rapid generation of light beams carrying orbital angular momentum," Opt. Express **21**(25), 30196–30203 (2013).
52. C. Schulze, D. Flamm, M. Duparré, and A. Forbes, "Beam-quality measurements using a spatial light modulator," Opt. Lett. **37**(22), 4687–4689 (2012).
53. K. Singh, N. Tabebordbar, A. Forbes, and A. Dudley, "Digital stokes polarimetry and its application to structured light: tutorial," JOSA A **37**(11), C33–C44 (2020).